THE JOURNAL OF PHYSICAL CHEMISTRY C

Article

pubs.acs.org/JPCC

First-Principles Investigation of Mercury Adsorption on the α-$Fe_2O_3(1\bar{1}02)$ Surface

Ji-Eun Jung,[†] Dawn Geatches,[†,∥] Kyoungjin Lee,[†] Shela Aboud,[†,⊥] Gordon E. Brown, Jr.,[‡,§] and Jennifer Wilcox*[,†]

[†]Department of Energy Resources Engineering, [‡]Department of Geological Sciences, and [§]Department of Chemical Engineering, Stanford University, 367 Panama Street, Stanford, California 94305-2220, United States

Supporting Information

ABSTRACT: Theoretical investigations using density functional theory (DFT) have been carried out to understand the interaction between mercury (Hg) and hematite (α-Fe_2O_3), both of which are released during the coal combustion processes. A clean α-$Fe_2O_3(1\bar{1}02)$ surface was chosen as a representative hematite model in this study based upon a previous *ab initio* thermodynamics study showing the high stability of this surface in the temperature range of typical flue gases. In order to determine the effect of chlorine (Cl) during Hg adsorption, the most probable adsorption sites of Hg, Cl, and HgCl on the clean α-Fe_2O_3 surface termination were found based on adsorption energy calculations, and the oxidation states of the adsorbates were determined by Bader charge analysis. Additionally, the projected density of states (PDOS) analysis characterizes the surface−adsorbate bonding mechanism. The adsorption energy of −0.103 eV indicates that Hg physisorbs to the clean α-Fe_2O_3 surface, and the subsequent Bader analysis confirms that the Hg becomes oxidized. Adding Cl to the Hg-adsorbed surface further enhances the strength of Hg adsorption, as evidenced by a shortened Hg−surface equilibrium distance. Bader charge and PDOS analyses also suggest that the presence of Cl enhances the charge transfer between the hematite surface and the adsorbate, thereby increasing the adsorption strength.

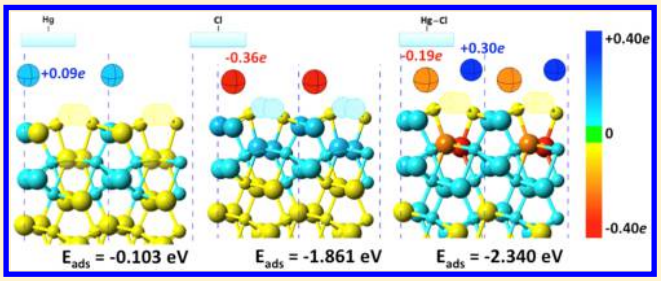

1. INTRODUCTION

Over 30% of today's overall global energy demands and over 40% of global electricity production are met by burning coal.[1] Despite its abundance and high capacity for energy generation, the continued use of coal is controversial from an environmental perspective. In particular, the emission of mercury (Hg) from coal-fired power plants is a critical environmental concern. Annually, 475 tons of Hg are released from coal-burning processes worldwide, comprising 24% of the total anthropogenic Hg emissions.[2] In the United States, more than 50% of anthropogenic Hg is released from coal-fired power plants.[3]

Mercury toxicity has been widely reported in the literature. For instance, methylmercury (CH_3Hg) is the most toxic form of mercury in the biogeochemical cycle.[4] A common route for its transformation is from elemental mercury (Hg^0) to oxidized mercury (Hg^{2+}) and then to the form of CH_3Hg^+ by sulfate- or iron-reducing bacteria.[4] Later, humans may be exposed through the consumption of contaminated fish and wildlife.[5] CH_3Hg affects the immune system, alters genetic and enzymatic systems, and can damage the nervous system of contaminated fish and wildlife and of those consuming them. Also, mercury chloride ($HgCl_2$) is the most common oxidized form of mercury and is corrosive to the human eyes, skin, and respiratory tract upon short-term exposure; $HgCl_2$ may also affect the kidneys upon longer or repeated exposure.[6] In addition, Hg^0 is less toxic than other forms of mercury such as CH_3Hg but can cause tremors, gingivitis, and excitability when its vapor is inhaled over a long period of time.[4] Hg^0 can be transported long distances in the atmosphere due to its low solubility, high volatility, and chemical inertness.[7] Due to the high toxicity of Hg species to humans, the Environmental Protection Agency (EPA) proposed standards on mercury and toxic air pollutants (mercury and air toxics standards, MATS)[3] in September 2011 for the new and existing coal- and oil-fired power plants.[8] These standards regulate the emissions of Hg, arsenic (As), selenium (Se), acid gases (e.g., hydrogen chloride (HCl) and hydrogen fluoride (HF)), and particulate matter (PM). Under MATS, 90% of Hg in coal-fired flue gas must be eliminated before being released from the stack with proper technologies.[3] EPA estimates $9.6 billon/year will be required to implement the relevant facilities, but this high cost has been an important factor in terms of implementation of MATS according to the very recent decision made by the U.S. Supreme Court in June 2015.[9] Therefore, cost-effective methods to control Hg emissions will be required to prevent further emissions.

To control the emission of Hg from coal-derived flue gas, it is important to understand the behavior and speciation of Hg from the boiler to the stack since the effectiveness of Hg capture

Received: August 11, 2015
Revised: October 23, 2015
Published: October 27, 2015

DOI: 10.1021/acs.jpcc.5b07827
J. Phys. Chem. C 2015, 119, 26512−26518

depends upon its speciation. In a coal-fired power plant, three types of Hg species exist. Gaseous Hg^0 is released at the boiler and mixed into the flue gas. During the cooling process from a high temperature of 1100 °C at the boiler exit to below 50 °C at the stack, Hg^0 can undergo speciation changes into oxidized forms such as Hg^{2+} (e.g., $HgCl_2$ and HgO) or a particulate form (Hg_p) where Hg^{2+} is adsorbed onto particulate matter (PM);[10] however, Hg^0 cannot be completely converted to Hg^{2+} or Hg_p because of its limited oxidation and adsorption efficiency. Compared to Hg^{2+} and Hg_p, which are easily removed from flue gas using wet flue gas desulfurization (WFGD) and electrostatic precipitators, respectively,[11] it is more difficult to eliminate Hg^0 due to its high vapor pressure and low solubility.[11,12] Therefore, enhancing oxidation of Hg^0 and sorption of Hg^{2+} on particle surfaces is a major concern in terms of Hg emission control in a coal-fired power plant.

The efficiency of Hg^0 oxidation or Hg^{2+} adsorption depends largely on boiler conditions such as temperature and pressure, coal type, the presence of other gases in the flue gas, and the presence of catalytic materials. In this paper, we focus on factors that influence the oxidation and adsorption of Hg, especially the effect of gases, particularly halogens, as well as the identification of catalytic materials.

Mercury oxidation in flue gas can occur by two different mechanisms: homogeneous (gas phase) and heterogeneous (gas−surface interactions).[8] Homogeneous gas-phase oxidation of Hg relies on the reaction between elemental Hg and halogen radicals. The Cl radicals from HCl or Cl_2 in flue gas, which are released from the coal, react with Hg to form oxidized Hg. However, this homogeneous oxidation of Hg by Cl in practical combustion systems is likely 10% or less.[8] Rather, heterogeneous oxidation is responsible for much of the Hg oxidation observed in coal combustion systems.[8,13]

One of the important factors in heterogeneous oxidation is the type of catalytic surface. Heterogeneous Hg oxidation has been achieved through various approaches including improved contact of Hg with solid substrates in the existing particulate control devices and in WFGD scrubbers, the addition of sorbents, and the use of catalytic pretreatment reactors.[14] In particular, Hg oxidation and capture is a cobenefit to existing pollutant control devices including selective catalytic reduction (SCR) units, which are primarily used for NO_x reduction.[15] Commercial SCR catalysts (e.g., V_2O_5−TiO_2) can oxidize Hg^0 to $HgCl_2$, thereby allowing easy removal of Hg^{2+} during the WFGD process.[15] In the absence of such SCR units, noble metal catalysts, e.g., gold (Au), platinum (Pt), and palladium (Pd), have been suggested for the oxidation of Hg.[10,11,16] Sorbent injection of activated carbon is another widely used method to oxidize and adsorb Hg.[17]

Even though activated carbon (AC) is the most popular sorbent in industry, its high cost and the large amount of waste associated with its use have raised economic and environmental issues. While fly ash can be a desirable additive to concrete, adding a secondary revenue for coal-fired power plants, the presence of AC in the ash prevents the concrete from meeting the freeze−thaw requirement, thus rendering AC-containing fly ash unusable.[18] Therefore, it may be beneficial if fly ash could be directly used as a sorbent for Hg removal in place of AC. Since fly ash already exists in coal-fired flue gas, its direct use would eliminate the need for an additional sorbent, thereby saving the associated costs. Indeed, fly ash has been known to remove Hg by adsorption as well as to promote Hg oxidation.[19] Among various components comprising fly ash, unburned carbon is thought to play an important role in Hg capture as a catalytic surface.[20] Additionally, several studies have shown that transition metal oxides in fly ash, such as ferric oxide (Fe_2O_3) and cupric oxide (CuO), have significant catalytic activity for Hg adsorption and oxidation.[21,22]

When fly ash is used for oxidation and adsorption of Hg and then used as a concrete additive, the stability of Hg bound on the ash surface is an important issue that should be confirmed. The adsorbed Hg could be released into the atmosphere and transported to the ground by rain if the adsorbed state becomes unstable. The changes in speciation of Hg associated with its interaction with fly ash components could affect its adsorption stability, but this is not yet fully understood. Therefore, this study aims to provide new insights about the interaction between Hg and fly ash components in order to enable the design of effective Hg capture technologies.

Theoretical studies using density functional theory (DFT) have been used to help understand the molecular-level mechanisms of Hg adsorption and oxidation in fly ash. Fly ash is a mixture of various metal oxides and unburned carbon, rendering the modeling of the entire mixture challenging. Instead, theoretical studies of the binding of Hg on different fly ash components have been conducted. These studies have elucidated the potential Hg binding mechanism to component surfaces and explained the effects of flue gas components, such as Cl_2, HCl, O_2, and SO_2, on Hg binding. In addition to these fly ash systems, various sorbents and oxidation catalysts have been studied by DFT-based computations. For example, Padak et al.[23,24] simulated halogen-embedded activated carbon surfaces for Hg adsorption computationally and showed that Hg binding energies increase with the addition of halogen atoms, in the order F > Cl > Br > I. Sasmaz and Wilcox[25] studied the CaO(100) surface, which represents Ca-based sorbents promoting Hg oxidation in WFGD processes. They reported that adsorption of HgCl, $HgCl_2$, and SO_2 on the CaO(100) surface at 0.125 ML is chemisorption. while the relatively low binding energy of Hg^0 on CaO(100) is consistent with a physisorption mechanism. Xiang et al.[26] studied Hg^0 adsorption on the O-terminated and Cu-terminated Cu(110) surface. They found that Hg physically adsorbed on the O-terminated Cu(110) surface and chemisorbed on the Cu-terminated surface. Compared to other studies[25,27] which stated Hg−O interactions are more favorable, this paper suggested the Hg atom binds to the Cu atom, which is evidenced by short bond length and strong adsorption energy for a specific configuration. A similar study tested Hg^0 adsorption on MnO_2(110)[28] and also investigated the stability of HgCl and $HgCl_2$ on the surface. They showed adsorbing behavior of HgCl both with Hg-down and Cl-down orientation as well as suggested the adsorption energy of $HgCl_2$ on the surface. Recently, Zhang et al.[29] have investigated heterogeneous Hg oxidation by HCl over a CeO_2 catalyst using DFT. They showed the entire Hg oxidation reaction pathway from Hg to HgCl and $HgCl_2$ and suggested that the formation of $HgCl_2$ is the rate-determining step.

In the present study, a DFT approach similar to the previous theoretical work described above has been applied to model the interaction of Hg with hematite (α-Fe_2O_3). A recent experimental study carried out by Jew et al.[30] revealed that α-Fe_2O_3 is the only metal oxide among the various chemical components in fly ash that binds Hg^{2+}. Also, Jew et al. found Fe-associated Hg-rich areas and showed a high spatial correlation of Hg with Fe and Cl (Figure S1). On the basis of their experimental results, our theoretical study of the interaction of Hg with fly ash

DOI: 10.1021/acs.jpcc.5b07827
J. Phys. Chem. C 2015, 119, 26512−26518

has focused on an α-Fe_2O_3 substrate. The high reactivity of the α-$Fe_2O_3(0001)$ surface toward metal adsorption has been discussed in the literature.[31−33] In contrast, there have been only a few studies of the interaction of Hg or other heavy metals with the α-$Fe_2O_3(1\bar{1}02)$ surface, which is known to be clean, chemically stable, well-ordered, and reactive toward Hg oxidation.[34−36] For example, Wasserman et al.[37] found a greater amount of hydroxylation for the $(1\bar{1}02)$ surface than for the (0001) surface both for gas-phase and solution-phase adsorption. Also, a previous study conducted by Lo et al.[38] and Aboud et al.[34] suggested that the α-$Fe_2O_3(1\bar{1}02)$ surface is thermodynamically stable in the presence of water and oxygen at the temperature and pressure conditions of the coal-fired flue gas environment.

To the best of our knowledge, this is the first theoretical study to examine Hg adsorption mechanisms on the α-$Fe_2O_3(1\bar{1}02)$ surface. Our specific goal is to investigate the adsorption of Hg on this surface in both the absence and presence of Cl derived from Cl_2 and HCl. We assumed that HCl will be dissociated in the flame to produce short-lived Cl radicals that will react with Hg in the gas phase to a minor extent, but primarily on a surface, such as the Fe-based surface studied in this work. Details of the structural and electronic properties of these systems have also been investigated.

2. COMPUTATIONAL METHODOLOGY

2.1. DFT Calculation Parameters. All DFT calculations were carried out using the Vienna *ab initio* Simulation Package (VASP) code.[39−42] The projector-augmented wave (PAW) method[43,44] was employed to represent the electron−ion interactions, and the electron exchange-correlation functional was represented by the generalized gradient approximation (GGA) with the model of Perdew, Burke, and Ernzerhof (PBE)[45,46] for nonlocal corrections. A kinetic energy cutoff of 450 eV was used for the plane-wave basis set. The integration of the Brillouin zone was conducted using a $5 \times 5 \times 5$ Monkhorst−Pack grid[47] including the Γ-point ($5 \times 5 \times 1$ for the surface), and Gaussian smearing was applied with a width of 0.2 eV. All atoms were fully relaxed and optimized until the atomic forces were less than 0.03 eV/Å.[34] The convergence criteria for the energy was set to 10^{-6} eV. To improve computational efficiency, a (1×1) unit cell was employed for all calculations with the energy convergence of 0.2 meV/atom. Additionally, spin polarization calculations were conducted to consider the magnetic moments of the individual Fe atoms, although bulk α-Fe_2O_3 has antiferromagnetic characteristics.

2.2. Slab Model Description. The α-$Fe_2O_3(1\bar{1}02)$ surfaces were constructed by cleaving the bulk α-Fe_2O_3 along the $(1\bar{1}2)$, $(1\bar{1}0)$, and $(1\bar{1}1)$ planes. Along the $[1\bar{1}2]$ direction, a double-sided slab model of α-Fe_2O_3 was constructed using the following unit cell parameters: a = 5.031 Å, b = 5.031 Å, and c = 13.753 Å. Compared to the experimental values,[48−50] the calculated DFT value in this paper is within 3.3%.[34] A vacuum region of 30 Å was introduced to minimize fictitious interactions between periodic images. The slab was formed with 21 atomic layers, which is thick enough to maintain the bulk structure in the center region of the slab.[34]

Figure 1 shows the oxygen-terminated $(1\bar{1}02)$ surface. The unit cell of the slab model consists of 42 atoms (16 Fe atoms and 26 O atoms). After geometry optimization, the layer spacings along the $[1\bar{1}02]$ direction were measured and compared to the previous DFT[34] and experimental[51] values to confirm the validity of the optimization.

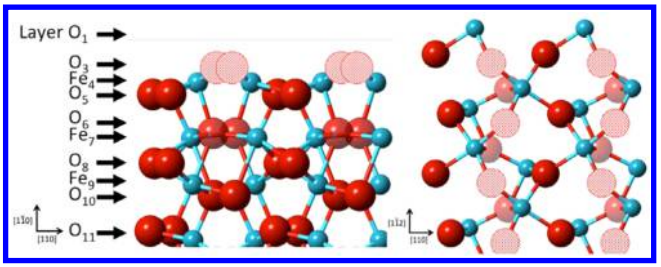

Figure 1. Side and top views of the α-$Fe_2O_3(1\bar{1}02)$ surface. Red and blue spheres denote oxygen and iron, respectively. The cross-hatched spheres denote the oxygen atoms terminating the surface (O_3 layer), and the lighter colored red atoms denote oxygen atoms in the subsurface (O_5 layer).

Because the hydrated α-$Fe_2O_3(1\bar{1}02)$ structure has a corrugated surface, there were various potential adsorption sites. To find the lowest energy configuration upon adsorption, total energy calculations were conducted for every possible site by relaxing the geometry of the entire slab. After all of the total energies were calculated, the configuration showing the strongest adsorption was determined to be the final adsorption configuration. The adsorption energy of each configuration was calculated by the following equation

$$E_{ads} = E_{slab+adsorbate} - E_{slab} - E_{gas\ phase}$$

where $E_{slab+adsorbate}$, E_{slab}, and $E_{gas\ phase}$ represent the total energies of the adsorbate on a slab, the clean slab, and the gas-phase atom (Hg or Cl) in the vacuum space, respectively.

2.3. Bader Charge and Projected Density of States (PDOS) Analyses. The electronic and charge properties of the adsorbates and α-$Fe_2O_3(1\bar{1}02)$ systems were investigated by analyzing the Bader charge[52] and PDOS. In Bader analysis, the electron charge distribution from the DFT calculation was partitioned and assigned to individual atoms. The differences in the partitioned charge before and after adsorption indicate charge transfer between the surface and adsorbate, thereby determining the oxidation or reduction characteristics of the adsorption process. PDOS analysis examines chemical bonding interactions by showing the changes in the occupation of the electron energy levels associated with adsorption.

3. RESULTS AND DISCUSSION

3.1. Optimized Geometries and Adsorption Energies of Hg, Cl, and HgCl on the α-$Fe_2O_3(1\bar{1}02)$ Surface. Every possible configuration of each adsorbate on the corrugated α-$Fe_2O_3(1\bar{1}02)$ surface was examined. For the cases of single Hg and Cl adsorption, 22 different initial configurations were examined (Figure S2). From the converged result of Hg adsorption using those initial configurations, we were able to find three major groups of configurations (see Table S1 and Figures S3 and S4). Among these configurations, the most stable Hg, Cl, and HgCl adsorption sites, which showed the lowest adsorption energies, are shown in Figure 2. The adsorption energy and equilibrium distance in each case are given in Table 1. The calculated adsorption energy of Hg is −0.103 eV, which indicates physisorption of Hg on the surface. The equilibrium distance of Hg−O is between 3.41 and 3.48 Å, and the Hg−Fe distance is 3.00 Å (Figure 2(a)). Although the equilibrium distance between Hg and Fe is closer than that between Hg and O, this is insufficient data to state definitively that Hg interacts with Fe directly. Rather, Hg is coordinated with four oxygen atoms in the two surface layers forming tetradentate structures.

DOI: 10.1021/acs.jpcc.5b07827
J. Phys. Chem. C 2015, 119, 26512−26518

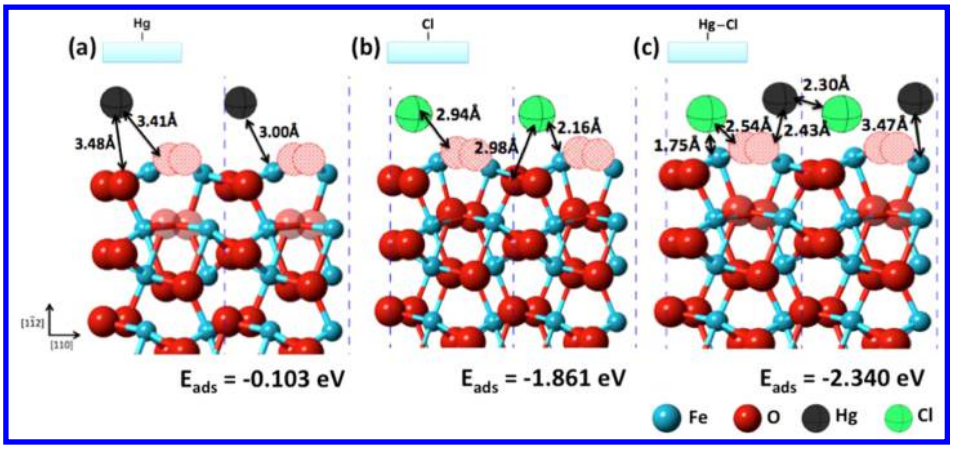

Figure 2. Stable configurations, equilibrium distances, and adsorption energies of Hg, Cl, and HgCl on the α-$Fe_2O_3(1\bar{1}02)$ surface. Numbers in the figure show equilibrium distances between the adsorbate and the surface.

Table 1. Adsorption Energies and Equilibrium Distances of Hg, Cl, and HgCl

	adsorption energy (eV)	equilibrium distance (Å)[a]		
		X–O	X–Fe	Hg–Cl
Hg	−0.103	3.41/3.48	3.00	-
Cl	−1.861	2.94/2.98	2.16	-
HgCl	−2.340	2.43(Hg–O)	3.47(Hg–Fe)	2.30
		2.54(Cl–O)	1.74(Cl–Fe)	

[a]X denotes an adsorbate in a given system (Hg or Cl).

Chlorine adsorption on the α-$Fe_2O_3(1\bar{1}02)$ surface was also investigated, with all unique initial configurations of a single Cl atom considered. Our results show that the most stable Cl adsorption site (Figure 2(b)) is another tetradentate structured site with four oxygen atoms. The equilibrium distance of Cl–O is 2.96 Å on average with a Cl–Fe distance of 2.16 Å; these distances are much closer than in the Hg-only configuration. The shorter equilibrium distances between the Cl atom and the surface compared to Hg are correlated with stronger adsorption energy (−1.861 eV), which is consistent with chemisorption. On the basis of these two results, Cl appears to be more reactive than Hg for the α-$Fe_2O_3(1\bar{1}02)$ surface.

In order to investigate the adsorption behavior of HgCl and the effect of Cl on the stability of Hg adsorbed on the surface, Cl was introduced to a Hg preadsorbed surface, identical to that of the configuration shown in Figure 2(a). In this case, Cl replaces the preadsorbed position of Hg and strongly adsorbs on the surface with shorter equilibrium distances compared to the singly adsorbed case (Figure 2(c)). The adsorption energy of HgCl on the surface is −2.340 eV, which is much stronger than both the Hg and Cl singly adsorbed cases.

3.2. Electronic Property Analysis. Results of the Bader charge analysis are shown in Figure 3 and Table 2, which represents the charge difference upon adsorption to the α-$Fe_2O_3(1\bar{1}02)$ surface. In the case of Hg adsorption, Hg and Fe atoms are positively charged, and O atoms are negatively charged, which is expected based on the electronegativity of each element. However, Hg becomes oxidized by donating electrons not only to the O atoms but also to the Fe atoms on the surface. This small electron transfer and the weak binding energy suggest a physisorption mechanism for Hg. In the case of the Cl-adsorbed α-$Fe_2O_3(1\bar{1}02)$ surface, Cl becomes reduced by gaining electron density from the surface atoms. The amount

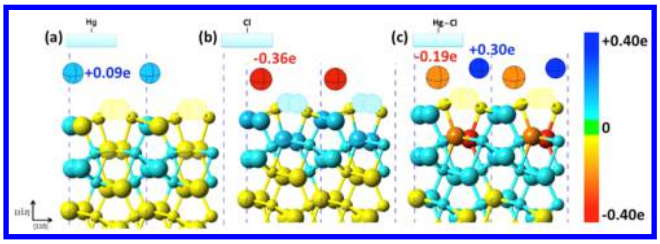

Figure 3. Results of the Bader charge analysis. All geometries are identical to those shown in Figure 2, with the color of the atoms denoting the extent of charge transferred during adsorption.

of transferred charge (−0.36*e*) is larger than in the Hg case (+0.09*e*), which confirms the strong adsorption energy of Cl compared to Hg on the α-$Fe_2O_3(1\bar{1}02)$ surface. When Cl was added to the Hg-adsorbed α-$Fe_2O_3(1\bar{1}02)$ surface, Hg donates more electron density to the surface (+0.30*e*) compared to the case of singly bound Hg (+0.09*e*). Even though Cl becomes less negatively charged than in the singly adsorbed Cl case (i.e., −0.19*e* and −0.36*e*, respectively), the total amount of transferred charge between the adsorbate and surface atoms is significantly larger than the singly adsorbed case. This result indicates that more active charge transfer occurred during the HgCl adsorption than in the Hg or Cl singly adsorbed cases.

The projected DOS analysis shows the occupation and energy distribution of each orbital. In Figure 4, PDOS plots of gas-phase Hg, the clean α-$Fe_2O_3(1\bar{1}02)$ surface, Hg-adsorbed surface, Cl-adsorbed surface, and HgCl-adsorbed surface are displayed. For each atom, the occupation of the Hg s-, O p-, Fe d-, and Cl p-states is displayed, as most correlations were observed within these densities of state. Fe and O of α-Fe_2O_3 are held together strongly through covalent bonding,[53] and this interaction is seen in Figure 4(b) by the overlapping Fe d-state and O p-state. Compared to the gas-phase Hg s-state, which has one peak around −0.5 eV (Figure 4(a)), the s-state of adsorbed Hg (Figure 4(c)) broadens and moves further away from the Fermi level to below the Fermi level upon adsorption. This shift indicates that Hg is slightly more stable in the adsorbed state than in the gas phase (Figure 4(c)). Examination of the peaks in Hg s-, Fe d-, and O p-states also suggests that electron densities overlap upon adsorption, which is further evidence of the Hg–Fe and Hg–O attractive interactions. However, considering that the Fe–O overlapped states do not change significantly upon Hg adsorption, and only a few s-states in Hg change upon

DOI: 10.1021/acs.jpcc.5b07827
J. Phys. Chem. C 2015, 119, 26512−26518

Table 2. Calculated Bader Charge Transfer upon Adsorption (Unit: *e*)[a]

	Hg	Cl	O1	O2	O3	O4	Fe1	Fe2
Hg adsorbed α-Fe_2O_3	0.09		−0.01	−0.02	0.00	0.00	−0.04	−0.01
Cl adsorbed α-Fe_2O_3		−0.36	0.06	0.07	0.07	0.05	−0.01	−0.02
HgCl adsorbed α-Fe_2O_3	0.30	−0.19	−0.02	−0.03	0.02	0.02	−0.15	−0.01

[a]O1−O4 and Fe1−Fe2 represent the label of the surface atom in the unit cell; see Figure S2.

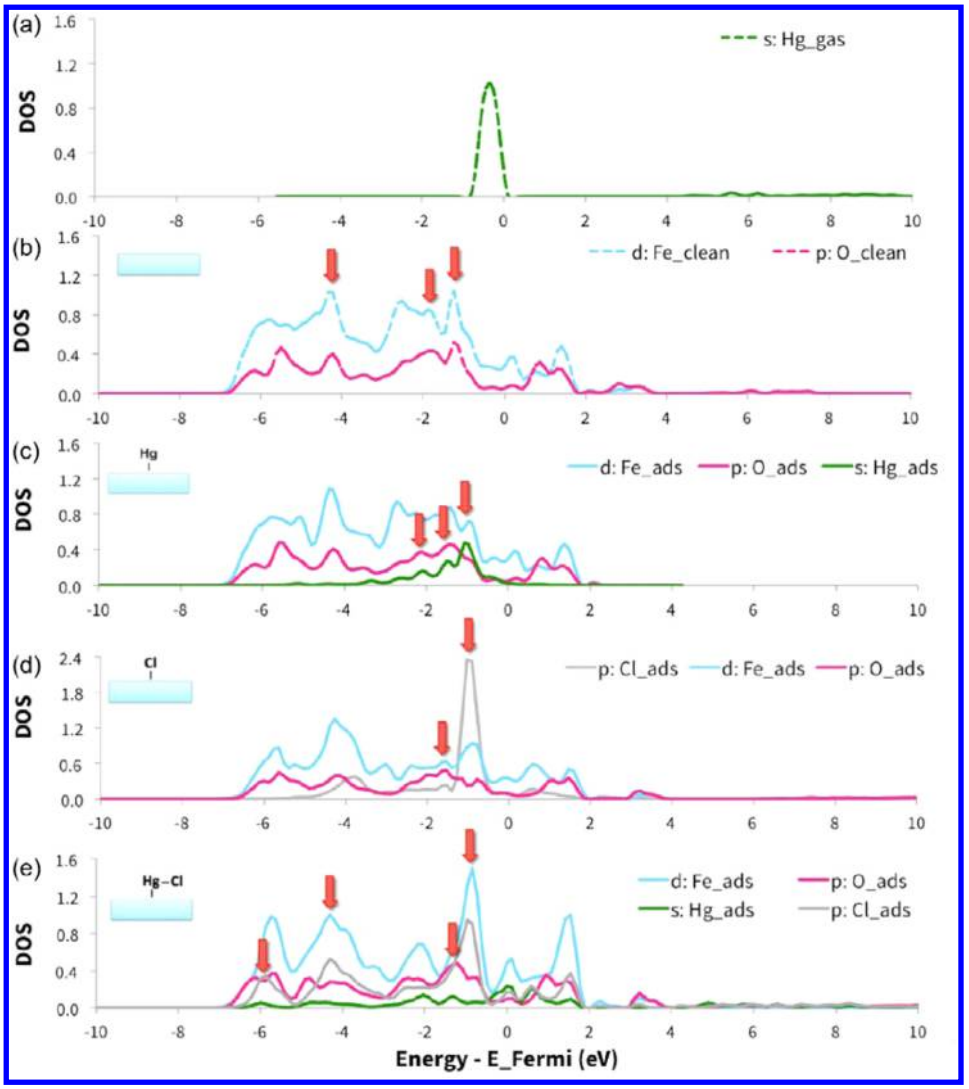

Figure 4. Projected densities of state (PDOS) of Hg, Cl, HgCl, and the α-$Fe_2O_3(1\bar{1}02)$ surface (a) gas-phase Hg, (b) Fe and O atom of the clean α-$Fe_2O_3(1\bar{1}02)$ surface, (c) Fe and O atoms adjacent to adsorbed Hg atom on the α-$Fe_2O_3(1\bar{1}02)$ surface, (d) Fe and O atoms adjacent to adsorbed Cl atom on the α-$Fe_2O_3(1\bar{1}02)$ surface, and (e) Fe and O atoms adjacent to adsorbed HgCl atoms on the α-Fe_2O_3 $(1\bar{1}02)$ surface. The Fermi level is referenced at 0 eV.

adsorption, these PDOS results are in reasonable agreement with the discussion of the Bader charge analysis, which implies physisorption of Hg. When Cl atoms are present on the surface, Fe d- and O p-states may be strongly hybridized with the Cl p-state as inferred from the characteristic overlaps in their DOSs, demonstrated in Figures 4(d) and 4(e). The overlap of the Fe d-, O p-, and Cl p-states during Cl adsorption strongly distorted the distribution of Fe d- and O p-states of the surface. This result is also in reasonable agreement with the large transfer of charge from the Cl atom to the surface O and Fe, as demonstrated from the Bader charge analysis. In the case of HgCl adsorption, the Hg s-state does not show significant hybridization with the surface atoms. In contrast, the overlap is evident between the Fe d-, O p-, and Cl p-states, which may indicate hybridization and chemical bonding between the Cl atom and the surface. This significant interaction of Cl with both the Fe and O atoms may strengthen the interaction between Hg and the α-Fe_2O_3 surface, thereby enhancing the adsorption energy of HgCl.

4. CONCLUSIONS

In this study, we have investigated stable configurations, adsorption energies, and electronic properties of Hg on the α-$Fe_2O_3(1\bar{1}02)$ surface. Hg weakly physisorbs to the surface with an adsorption energy of −0.103 eV. However, stronger adsorption strength, as well as the larger amount of transferred charge, indicates that Cl adsorbs on the surface more strongly

DOI: 10.1021/acs.jpcc.5b07827
J. Phys. Chem. C 2015, 119, 26512−26518

compared to Hg. Also, in the presence of Cl, Hg adsorption on α-Fe_2O_3 is strengthened compared to single Hg adsorption, evidenced by the shorter equilibrium distance between Hg and the surface, the larger amount of transferred charge, and overlaps of DOS. From these results, we suggest that halogens, especially Cl, play an important role in Hg adsorption onto α-Fe_2O_3. This result is consistent with experimental results,[30] which found a Hg−Fe−Cl relationship in fly ash. Weakly bound Hg can be strongly adsorbed with the help of Cl.

As this study does not consider transition states, it will be important to reveal the entire mechanism of adsorption in this system in a future study. Also, there is a discrepancy between the calculated equilibrium distances of Hg−Fe and Hg−O and those determined experimentally,[30] which are much shorter than those resulting from the DFT calculations. This inconsistency may be due to the approximations used in our DFT calculations, which deal with clean (i.e., no other gases) surfaces with limited surface coverage. In spite of the simplification of the system considered in this study, however, strong adsorption of Hg on the α-$Fe_2O_3(1\bar{1}02)$ surface is indicated in the presence of Cl. The results of the present investigation provide motivation for optimized Hg removal processes in a coal-fired power plant, and they also provide guidance for future studies of the possibility of Hg re-emission in natural systems.

■ ASSOCIATED CONTENT

Supporting Information

The Supporting Information is available free of charge on the ACS Publications website at DOI: 10.1021/acs.jpcc.5b07827.

Synchrotron X-ray fluorescence (s-XRF) maps of Fe-associated Hg region in the fly ash; possible Hg and Cl adsorption sites for α-Fe_2O_3 $(1\bar{1}02)$ surface; the adsorption configurations of Hg on α-Fe_2O_3 $(1\bar{1}02)$ surface, label of the surface atom for the Bader charge analysis results; and adsorption energies of Hg from 22 initial configurations are provided in the Supporting Information (PDF)

■ AUTHOR INFORMATION

Corresponding Author

*E-mail: wilcoxj@stanford.edu. Phone: (650) 724-9449. Fax: (650) 725-2099.

Present Addresses

[‖]Hartree Centre, STFC Daresbury Laboratory, Warrington, WA4 4AD, UK.

[⊥]Synopsis, 690 East Middlefield Road, Mountain View, CA 94043, USA.

Notes

The authors declare no competing financial interest.

■ ACKNOWLEDGMENTS

This work was supported by National Science Foundation combustion grant (CBET-1235879). The computational resources were supported by the National Science Foundation (TG-CHE100005) through Stampede systems provided by Texas Advanced Computing Center (TACC) and in part by the supercomputing cluster of the Center for Computational Earth & Environmental Sciences (CEES) at Stanford University. We would also like to thank Dr. Charles- François Pedro de Lannoy and Dr. Peter Psarras for their careful reviews of the manuscript.

■ REFERENCES

(1) IEA 21st Century Coal: Advanced Technology and Global Energy Solution; IEA/OECD: Paris, 2013; p 122.

(2) UNEP, Global Mercury Assessment 2013: Sources, Emissions, Releases and Environmental Transport. 2013.

(3) EPA, Mercury and Air Toxics Standards. 2012.

(4) USGS, Mercury in the Environment. http://www.usgs.gov/themes/factsheet/146-00/index.html.

(5) Morel, F. M. M.; Kraepiel, A. M. L.; Amyot, M. The Chemical Cycle and Bioaccumulation of Mercury. *Annu. Rev. Ecol. Syst.* **1998**, *29*, 543−566.

(6) IPCS, International Chemical Safety Cards. In ISCS: 0979: 1993.

(7) Chang, R.; Offen, G. R. Mercury Emission Control Technologies: an EPRI Synopsis. *Power Eng.* **1995**, *99*, 51.

(8) Wilcox, J.; Rupp, E.; Ying, S. C.; Lim, D.-H.; Negreira, A. S.; Kirchofer, A.; Feng, F.; Lee, K. Mercury Adsorption and Oxidation in Coal Combustion and Gasification Processes. *Int. J. Coal Geol.* **2012**, *90−91*, 4−20.

(9) U.S. Supreme Court, Decision on MATS. http://www.supremecourt.gov/opinions/14pdf/14-46_10n2.pdf.

(10) Presto, A. A.; Granite, E. J. Noble Metal Catalysts for Mercury Oxidation in Utility Flue Gas. *Platinum Met. Rev.* **2008**, *52*, 144−154.

(11) Presto, A. A.; Granite, E. J. Survey of Catalysts for Oxidation of Mercury in Flue Gas. *Environ. Sci. Technol.* **2006**, *40*, 5601−5609.

(12) Galbreath, K. C.; Zygarlicke, C. J. Mercury Speciation in Coal Combustion and Gasification Flue Gases. *Environ. Sci. Technol.* **1996**, *30*, 2421−2426.

(13) Granite, E. J.; Pennline, H. W.; Senior, C. *Mercury Control: for Coal-Derived Gas Streams*; John Wiley & Sons: New York, 2015; p 480.

(14) Niksa, S.; Fujiwara, N. A Predictive Mechanism for Mercury Oxidation on Selective Catalytic Reduction Catalysts under Coal-Derived Flue Gas. *J. Air Waste Manage. Assoc.* **2005**, *55*, 1866−1875.

(15) Negreira, A. S.; Wilcox, J. DFT Study of Hg Oxidation Across Vanadia-Titania SCR Catalyst Under Flue Gas Conditions. *J. Phys. Chem. C* **2013**, *117*, 1761−1772.

(16) Zhao, Y. X.; Mann, M. D.; Pavlish, J. H.; Mibeck, B. A. F.; Dunham, G. E.; Olson, E. S. Application of Gold Catalyst for Mercury Oxidation by Chlorine. *Environ. Sci. Technol.* **2006**, *40*, 1603−1608.

(17) Zhao, Y. C.; Zhang, J. Y.; Liu, J.; Diaz-Somoano, M.; Martinez-Tarazona, M. R.; Zheng, C. G. Study on Mechanism of Mercury Oxidation by Fly Ash from Coal Combustion. *Chin. Sci. Bull.* **2010**, *55*, 163−167.

(18) Miller, C. E.; Thomas J. Feeley, I.; Aljoe, W. W.; Lani, B. W.; Schroeder, K. T.; Kairies, C.; McNemar, A. T.; Jones, A. P.; Murphy, J. T. *Mercury Capture and Fate using Wet FGD at Coal-Fired Power Plants*; DOE/NETL Mercury and Wet FGD R&D: August, 2006.

(19) Bhardwaj, R.; Chen, X.; Vidic, R. D. Impact of Fly Ash Composition on Mercury Speciation in Simulated Flue Gas. *J. Air Waste Manage. Assoc.* **2009**, *59*, 1331−1338.

(20) Pavlish, J. H.; Sondreal, E. A.; Mann, M. D.; Olson, E. S.; Galbreath, K. C.; Laudal, D. L.; Benson, S. A. Status Review of Mercury Control Options for Coal-fired Power Plants. *Fuel Process. Technol.* **2003**, *82*, 89−165.

(21) Ghorishi, S. B.; Lee, C. W.; Jozewicx, W. S.; Kilgroe, J. D. Effects of Fly Ash Transition Metal Content and Flue Gas HCl/SO_2 Ratio on Mercury Speciation in Waste Combustion. *Environ. Eng. Sci.* **2005**, *22*, 221−231.

(22) Dunham, G. E.; DeWall, R. A.; Senior, C. L. Fixed-Bed Studies of the Interactions Between Mercury and Coal Combustion Fly Ash. *Fuel Process. Technol.* **2003**, *82*, 197−213.

(23) Padak, B.; Brunetti, M.; Lewis, A.; Wilcox, J. Mercury Binding on Activated Carbon. *Environ. Prog.* **2006**, *25*, 319−326.

(24) Padak, B.; Wilcox, J. Understanding Mercury Binding on Activated Carbon. *Carbon* **2009**, *47*, 2855−2864.

(25) Sasmaz, E.; Wilcox, J. Mercury Species and SO_2 adsorption on CaO(100). *J. Phys. Chem. C* **2008**, *112*, 16484−16490.

(26) Xiang, W.; Liu, J.; Chang, M.; Zheng, C. The Adsorption Mechanism of Elemental Mercury on CuO(110) Surface. *Chem. Eng. J.* **2012**, *200−202*, 91−96.

DOI: 10.1021/acs.jpcc.5b07827
J. Phys. Chem. C 2015, 119, 26512−26518

(27) Guo, P.; Guo, X.; Zheng, C. Roles of γ-Fe_2O_3 in Fly Ash for Mercury Removal: Results of Density Functional Theory Study. *Appl. Surf. Sci.* **2010**, *256*, 6991−6996.
(28) Zhang, B.; Liu, J.; Zheng, C.; Chang, M. Theoretical Study of Mercury Species Adsorption Mechanism on MnO_2(110) Surface. *Chem. Eng. J.* **2014**, *256*, 93−100.
(29) Zhang, B.; Liu, J.; Shen, F. Heterogeneous Mercury Oxidation by HCl over CeO_2 Catalyst: Density Functional Theory Study. *J. Phys. Chem. C* **2015**, *119*, 15047−15055.
(30) Jew, A. D.; Rupp, E. C.; Geatches, D. L.; Jung, J.; Farfan, G.; Bahet, L.; Hower, J. C.; Brown, G. E., Jr.; Wilcox, J. Mercury Interaction with the Fine Fraction of Coal-Combustion Fly Ash in a Simulated Coal Power Plant Flue Gas Stream. *Energy Fuels* **2015**, *29*, 6025−6038.
(31) Catti, M.; Valerio, G.; Dovesi, R. Theoretical Study of Electronic, Magnetic, and Structural Properties of Hematite. *Phys. Rev. B: Condens. Matter Mater. Phys.* **1995**, *51*, 7441−7450.
(32) Rollmann, G.; Rohrbach, A.; Entel, P.; Hafner, J. First-Principles Calculation of the Structure and Magnetic Phases of Hematite. *Phys. Rev. B: Condens. Matter Mater. Phys.* **2004**, *69*, 165107.
(33) Cornell, R. M.; Schwertmann, U. *The Iron Oxides: Structure, Properties, Reactions, Occurrences, and Uses*; Wiley-VCH: Weinhein, 2003.
(34) Aboud, S.; Wilcox, J.; Brown, G. E., Jr. Density Functional Theory Investigation of the Interaction of Water with α-Al_2O_3 and α-Fe_2O_3 (1n02) Surfaces: Implications for Surface Reactivity. *Phys. Rev. B: Condens. Matter Mater. Phys.* **2011**, *83*, 125407.
(35) Trainor, T. P.; Templeton, A. S.; Eng, P. J. Structure and Reactivity of Environmental Interfaces: Application of Grazing Angle X-ray Spectroscopy and Long-Period X-ray Standing Waves. *J. Electron Spectrosc. Relat. Phenom.* **2006**, *150*, 66−85.
(36) Mason, S. E.; Iceman, C. R.; Tanwar, K. S.; Trainor, T. P.; Chaka, A. M. Pb(II) Adsorption on Isostructural Hydrated Alumina and Hematite (0001) Surfaces: A DFT Study. *J. Phys. Chem. C* **2009**, *113*, 2159−2170.
(37) Wasserman, E.; Rustad, J. R.; Felmy, A. R.; Hey, B. P.; Halley, J. W. Ewald Methods for Polarizable Surfaces with Application to Hydroxylation and Hydrogen Bonding on the (012) and (001) Surfaces of α-Fe_2O_3. *Surf. Sci.* **1997**, *385*, 217−239.
(38) Lo, C.; Tanwar, K.; Chaka, A.; Trainor, T. Density Functional Theory Study of the Clean and Hydrated Hematite ($1\bar{1}02$) Surfaces. *Phys. Rev. B: Condens. Matter Mater. Phys.* **2007**, *75*, 075425.
(39) Kresse, G.; Furthmuller, J. Efficiency of Ab-Initio Total Energy Calculations for Metals and Semiconductors Using a Plane-Wave Basis Set. *Comput. Mater. Sci.* **1996**, *6*, 15−50.
(40) Kresse, G.; Furthmuller, J. Efficient Iterative Schemes for Ab Initio Total-Energy Calculations Using a Plane-Wave Basis Set. *Phys. Rev. B: Condens. Matter Mater. Phys.* **1996**, *54*, 11169.
(41) Kresse, G.; Hafner, J. Ab Initio Molecular Dynamics for Open-Shell Transition Metals. *Phys. Rev. B: Condens. Matter Mater. Phys.* **1993**, *48*, 13115.
(42) Kresse, G.; Hafner, J. Ab Initio Molecular-Dynamics Simulation of the Liquid-Metal-Amorphous-Semiconductor Transition in Germanium. *Phys. Rev. B: Condens. Matter Mater. Phys.* **1994**, *49*, 14251.
(43) Kresse, G.; Joubert, D. From Ultrasoft Pseudopotentials to the Projector Augmented-Wave Method. *Phys. Rev. B: Condens. Matter Mater. Phys.* **1999**, *59*, 1758.
(44) Blochl, P. E. Projector Augmented-Wave Method. *Phys. Rev. B: Condens. Matter Mater. Phys.* **1994**, *50*, 17953−17979.
(45) Perdew, J. P.; Burke, K.; Ernzerhof, M. Generalized Gradient Approximation Made Simple. *Phys. Rev. Lett.* **1996**, *77*, 3865−3868.
(46) Perdew, J. P.; Burke, K.; Ernzerhof, M. Erratum: Generalized Gradient Approximation Made Simple. *Phys. Rev. Lett.* **1997**, *78*, 1396.
(47) Monkhorst, H. J.; Pack, J. D. Special Points for Brillouin-Zone Integrations. *Phys. Rev. B* **1976**, *13*, 5188−5192.
(48) Kren, E.; Szabo, P.; Konczos, G. Neutron Diffraction Studies on the (1−x) Fe_2O_3 − xRh_2O_3 System. *Phys. Lett.* **1965**, *19*, 103−104.
(49) Sarma, D. D.; Shanthi, N.; Barman, S. R.; Hamada, N.; Sawada, H.; Terakura, K. Band Theory for Ground-State Properties and Excitation Spectra of Perovskite $LaMO_3$ (M= Mn, Fe, Co, Ni). *Phys. Rev. Lett.* **1995**, *75*, 1126.
(50) Coey, J. M. D.; Sawatzky, G. A. A Study of Hyperfine Interactions in the System $(Fe_{1-x}Rh_x)_2O_3$ Using the Mossbauer Effect (Bonding Parameters). *J. Phys. C: Solid State Phys.* **1971**, *4*, 2386.
(51) Tanwar, K. S.; Lo, C. S.; Eng, P. J.; Catalano, J. G.; Walko, D. A.; Brown, G. E.; Waychunas, G. A.; Chaka, A. M.; Trainor, T. P. Surface Diffraction Study of the Hydrated Hematite Surface. *Surf. Sci.* **2007**, *601*, 460−474.
(52) Henkelman, G.; Arnaldsson, A.; Jónsson, H. A Fast and Robust Algorithm for Bader Decomposition of Charge Density. *Comput. Mater. Sci.* **2006**, *36*, 354−360.
(53) Blake, R. L.; Hessevick, R. E.; Zoltai, T.; Finger, L. W. Refinement of the Hematite Structure. *Am. Mineral.* **1966**, *51*, 123−129.

DOI: 10.1021/acs.jpcc.5b07827
J. Phys. Chem. C 2015, 119, 26512−26518